Journal of Marine Research, *59*, 391–416, 2001

Observations of the wind-induced exchange at the entrance to Chesapeake Bay

by Arnoldo Valle-Levinson[1], Kuo-Chuin Wong[2] and Kathryn T. Bosley[3]

ABSTRACT

Water density and velocity data from two ~75-day deployments across the entrance to the Chesapeake Bay were used in conjunction with wind velocity and sea level records to describe the transverse structure of wind-induced subtidal exchange. Acoustic Doppler current profilers, electromagnetic current meters, and conductivity-temperature-depth recorders were deployed at the entrance to the bay from mid-April to early July of 1999 and from early September to mid-November of 1999. Three main scenarios of wind-induced exchange were identified: (1) Northeasterly (NE) winds consistently drove water from the coast toward the lower Chesapeake Bay as well as water from the upper bay to the lower bay, which was indicated by the surface elevation slopes across the lower bay and along the bay. This resulted in water piling up against the southwestern corner of the bay. The subtidal flow over the southern portion of the bay entrance was directed to the left of the wind direction, likely the result of the influence of Coriolis and centripetal accelerations on the adjustment of the sea level gradients. Over the northern shallow half of the entrance, the subtidal flows were nearly depth-independent and in the same direction as the wind. (2) Southwesterly (SW) winds caused opposite sea level gradients (relative to NE winds), which translated into near-surface outflows throughout the entrance and near-bottom inflows restricted to the channels. This wind-induced circulation enhanced the two-way exchange between the estuary and the adjacent ocean. (3) Northwesterly winds produced the same exchange pattern as NE winds. Water piled up against the southwestern corner of the bay causing net outflow in the deep, southern area and downwind flow over the shallow areas. Northwesterly winds greater than 12 m/s caused the most efficient flushing of the bay, driving water out over the entire mouth of the estuary.

1. Introduction

The effect of wind forcing on the subtidal variability in estuaries has been known for some time (e.g. Pollak, 1960). Weisberg and Sturges (1976) and Weisberg (1976) found that the subtidal circulation in the Providence River and the west passage of Narragansett Bay was dominated by wind-induced fluctuations. In a series of studies related to Chesapeake Bay and some of its tributary estuaries, Wang and Elliott (1978), Elliott

1. Center for Coastal Physical Oceanography, Department of Ocean, Earth and Atmospheric Sciences, Old Dominion University, Norfolk, Virginia, 23529, U.S.A. ***email: arnoldo@ccpo.odu.edu***

2. College of Marine Studies, University of Delaware, Newark, Delaware, 19716, U.S.A.

3. National Ocean Service, National Oceanic and Atmospheric Administration, Crittenton Hall, 768 W. 52nd Street, Norfolk, Virginia, 23529, U.S.A.

(1978), and Wang (1979a,b) showed that the dominant subtidal sea level fluctuations in Chesapeake Bay were the result of up-bay propagation of coastal sea level fluctuations generated by alongshore winds. They also found that the subtidal barotropic volume exchange in the lower bay was part of the response of the coupled bay-shelf system to atmospheric forcing. The importance of wind forcing on low frequency estuarine variability has also been demonstrated by studies conducted by Smith (1977, 1978) in Corpus Christi Bay, Texas and Kjerfve *et al.* (1978) in North Inlet, South Carolina.

The nature and characteristics of the wind-induced subtidal variability has been examined in different types of estuaries. These include partially mixed estuaries such as Chesapeake Bay (Vieira, 1985, 1986; Goodrich *et al.,* 1987, Goodrich, 1988; Chuang and Boicourt, 1989; Valle-Levinson, 1995; Paraso and Valle-Levinson, 1996; Valle-Levinson and Lwiza, 1998), San Francisco Bay (Walters, 1982; Walters and Gartner, 1985), and Delaware Bay (Wong and Garvine, 1984; Wong, 1994); as well as shallow but highly stratified estuaries such as Mobile Bay (Schroeder and Wiseman, 1986; Wiseman *et al.,* 1988; Noble *et al.,* 1996) and the Childs and Quashnet in Massachusetts' Waquoit Bay (Geyer, 1997). Furthermore, wind forcing has also been shown to be important to the subtidal exchange in many coastal lagoons with restricted communication with the ocean (e.g. Wong and Wilson, 1984, Kjerfve and Knoppers, 1991).

Despite the extensive literature on the subject of subtidal exchange between an estuary and the continental shelf, many fundamental questions remain unresolved due to a lack of observational data with sufficient spatial resolution of the wind-induced exchange. For example, what is the basic pattern of local wind-induced currents in a coastal plain estuary with lateral variation in bathymetry? Does it vary primarily in the vertical dimension, with downwind current in the upper layer and upwind current in the lower layer, or does it exhibit substantial lateral variability? How does the lateral variation in the current velocity correlate with the change in bathymetry across the estuary? It is timely to address some of these issues as they are crucial to elucidate the effect of wind on subtidal exchange between an estuary and the adjacent continental shelf.

There have been different approaches to examine the magnitude and spatial characteristics of the wind-induced volume exchange in estuaries. In idealized estuaries with simple lateral depth variations, several analytical and numerical modeling studies (e.g. Csanady, 1973; Wong, 1994; Signell *et al.,* 1990; Glorioso and Davies, 1995; Friedrichs and Hamrick, 1996; Hunter and Hearn, 1987; Hearn *et al.,* 1987) and a laboratory study (Fischer, 1976) showed that a downwind current exists throughout the water column over the shallow areas along the shores and an upwind return flow develops mainly in the deep channel. In these studies the downwind flow along the shores canceled the upwind flow in the channel, resulting in zero (or weak) sectionally averaged barotropic current. These idealized results have not been fully corroborated by observations, which is the intent of this study.

The ultimate goal of this study is to advance our knowledge of the wind-induced estuary-shelf subtidal exchange. The specific objective of this work is to document the

magnitude and spatial characteristics of the wind-induced volume exchange between a major estuary (Chesapeake Bay) and the adjacent continental shelf. This objective is accomplished by analysis of time series measurements of water velocity profiles, near-surface and near-bottom water density, wind velocity and sea level at different locations across the entrance to the Chesapeake Bay.

2. Study area

The study area at the entrance to the Chesapeake Bay represents a typical wide (width greater than the internal radius of deformation) partially mixed coastal plain estuary. Physical oceanographic processes in the lower Chesapeake Bay are chiefly influenced by wind, tidal, and buoyancy forcing as well as by the bathymetry. The bathymetry at the entrance to the bay is characterized by two channels, the Chesapeake Channel that extends to depths of 30 m, and the North Channel, of maximum depth of 14 m (Fig. 1). These channels are found near the southern and northern end of the entrance to the bay, respectively. The channels are separated by Middle Ground, which is a relatively flat region of ~10 m depth found immediately to the north of Chesapeake Channel, and the Six-Meters Shoal, immediately to the south of the North Channel.

Wind forcing in the lower Chesapeake Bay is seasonal and primarily from the northeast and the southwest directions (Paraso and Valle-Levinson, 1996). Northeasterly winds prevail from late summer to early spring, while southwesterly winds dominate during the summer. The most energetic wind events are usually from the northeast or northwest during late fall and winter, although energetic southwesterly winds can occasionally be observed.

Tidal forcing in the lower Chesapeake Bay is predominantly semidiurnal (Browne and Fisher, 1988). The interaction among the three semidiurnal tidal constituents (M_2, N_2 and S_2) generates fortnightly and monthly variability in the tidal currents. There is a marked asymmetry between consecutive spring (or neap) tides that delineates a primary and a secondary spring (or neap) tide during one month. This asymmetry is the result of the N_2 constituent dominating over the S_2 in the lower bay. During spring tides, the currents in the lower bay may exceed 1 m/s.

Buoyancy forcing to the lower Chesapeake Bay is dominated by river discharge. River discharge to the bay is mostly (~80% of the total) represented by three rivers: Susquehanna, Potomac and James. Discharge peaks during March and April and is least during August and September. As a result, the mean surface salinity is lowest throughout the bay in the April-May period and highest in September-November, roughly one month after the river discharge extremes. The mean discharge into the bay is ~2500 m^3/s (Goodrich, 1988). Although high buoyancy forcing for the spring-summer period and low buoyancy forcing for the autumn period were expected, moderate buoyancy forcing existed during the entire study period (see Section 4).

Characterization of exchange flows at different times of the year has been done at high spatial resolution in the study area using short-term (1 day) Acoustic Doppler Current

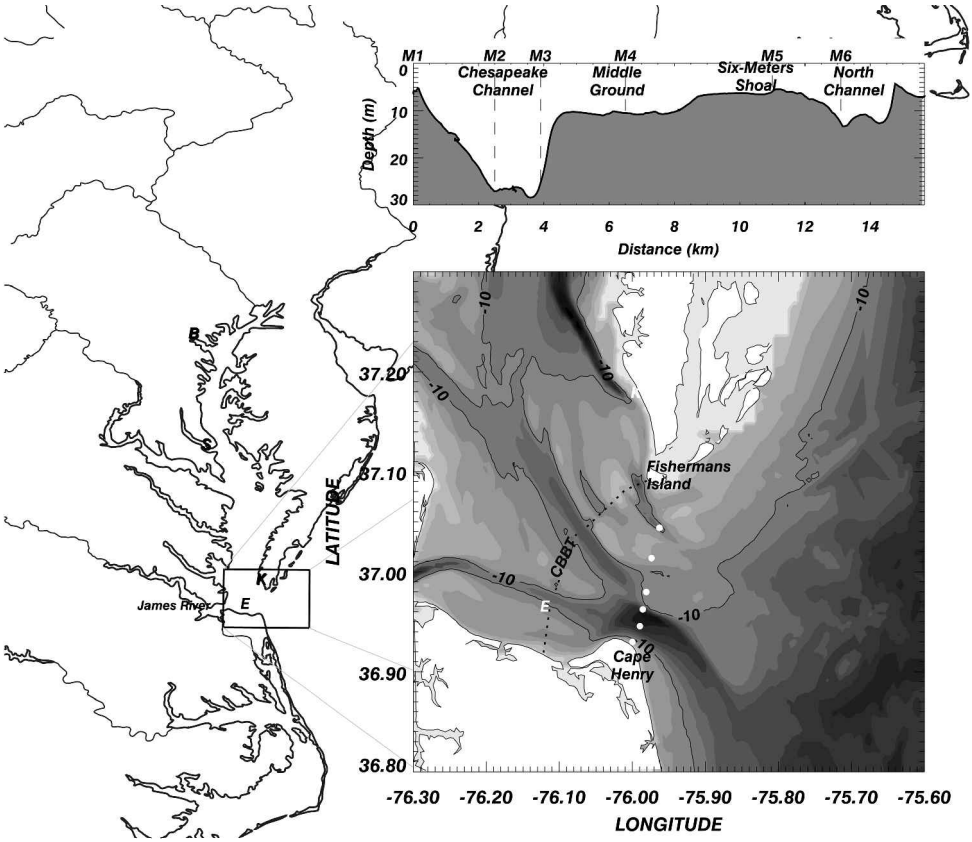

Figure 1. Map of the study area showing the lower Chesapeake Bay in the context of the eastern United States. The bathymetry of the lower Chesapeake Bay is shown with filled contours for which the darker tones denote deeper areas and with the 10 m isobath drawn for reference. The mooring locations are indicated by the small white circles at the entrance to the bay. The bathymetry of the sampling transect is shown in the upper insert with the appropriate labels for the bathymetric features discussed in the text and the corresponding position of the moorings M1, M2, M3, M4, M5, and M6. The location of the CBBT, Kiptopeke, Solomons Island, and Baltimore sensors are denoted by E, K, S, and B, respectively on the map that shows the entire Chesapeake Bay.

Profiler (ADCP) tows (Valle-Levinson *et al.,* 1998). That study identified two main scenarios of water exchange modified by wind: a southwesterly wind scenario and a nonsouthwesterly wind scenario (Fig. 2). In the nonsouthwesterly wind scenario, which may be considered as the typical or density-dominated exchange, gravitational circulation was observed in the Chesapeake and North channels and a tidally induced residual recirculation was found around the Six-Meters Shoal. In the southwesterly wind scenario, wind forcing enhances the gravitational circulation in the channels and produces a net outflow in place of the recirculation over the Six-Meters Shoal. These two scenarios were

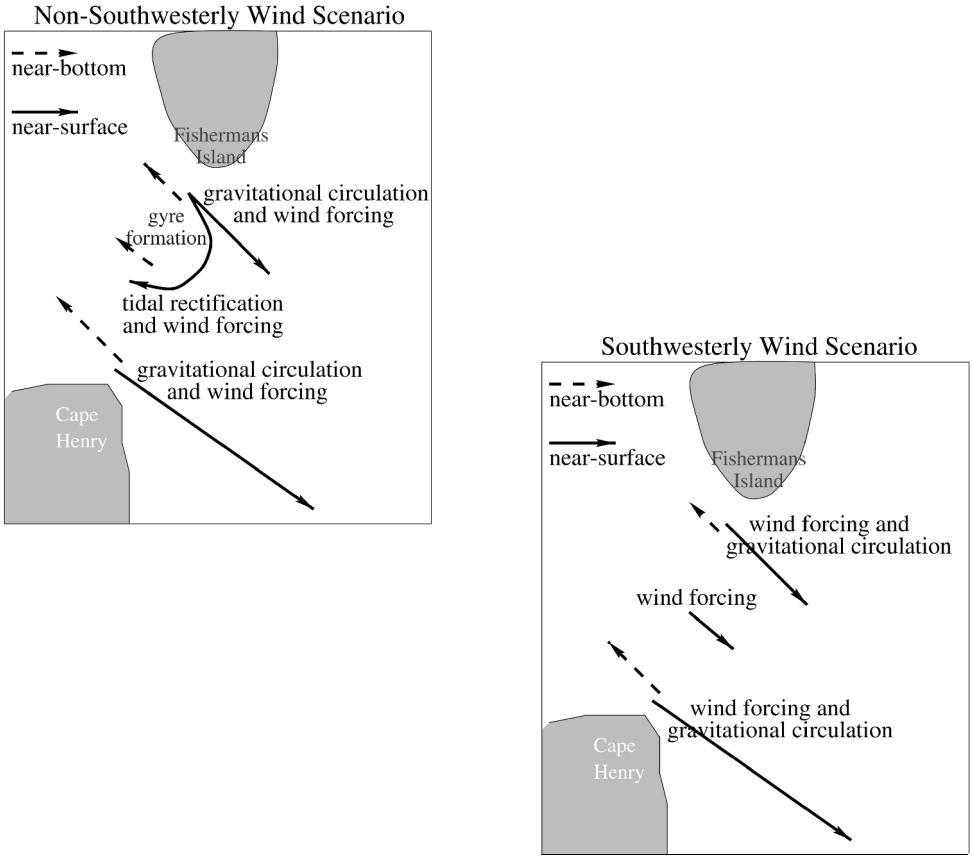

Figure 2. Water exchange scenarios proposed by Valle-Levinson *et al.* (1998) as derived from high spatial resolution but low temporal resolution sampling. Continuous vectors represent near-surface velocities and dashed vectors represent near-bottom velocities.

drawn from short time series and under relatively weak (<10 m/s) wind forcing conditions. Therefore, the two scenarios fail to reflect the characteristics of the water exchange under strong and variable wind forcing conditions. The long-term deployments presented here allow refinements to the scenarios drawn from those short-term data sets and permit the portrayal of new scenarios that depend on different wind conditions.

3. Data collection

Two ~75-day deployments of moored instrumentation were carried out in the spring-summer and in the autumn of 1999. Instrumentation deployed consisted of five upward-looking bottom-mounted Acoustic Doppler Current Profilers (ADCPs) with pressure sensors, three point current-meters, and six conductivity-temperature-depth recorders. This instrumentation was distributed in six moorings as shown in Table 1.

Table 1. Details on each instrument deployment. Times are given in GMT. The Dep1 column indicates the total water column depth. The Dep2 column indicates the depth at which the instrument was deployed. All instruments recorded at 15 minute-ensembles. ADCPs recorded 200 pings per ensemble.

	Mooring	Instrument	Latitude (N)	Longitude (W)	Day & Time in	Dep1 (m)	Dep2 (m)
Spring-	2	CT/SBE-26	36° 57.1559′	76° 01.4018′	20/04/99 1350	18.3	2
	2	CT/SBE-37	36° 57.1559′	76° 01.4018′	20/04/99 1330	18.3	17
Summer	4	CT/SBE-37	36° 57.8317′	75° 59.5507′	20/04/99 1718	24.4	2
	4	CT/SBE-37	36° 57.8317′	75° 59.5507′	20/04/99 1705	24.4	23
Deployment	6	CT/SBE-26	37° 02.56′	75° 57.32′	19/04/99 1830	10.4	2
	6	CT/SBE-37	37° 02.56′	75° 57.32′	19/04/99 1820	10.4	9
April–July	1	ADCP/WH-1200	36° 55.7891′	75° 59.9946′	20/04/99 1645	7.3	7
	2	ADCP/WH-600	36° 56.7269′	75° 59.3762′	20/04/99 1736	23.5	23
1999	3	ADCP/WH-300	36° 57.7378′	75° 59.1358′	19/04/99 2129	22.9	22.5
	4	ADCP/WH-600	36° 58.7881′	75° 58.8509′	22/04/99 1315	10.4	10
	5	S4	37° 00.8090′	75° 58.4200′	19/04/99 1605	6.7	3
	5	S4	37° 00.8090′	75° 58.4200′	21/04/99 1500	6.7	5
	6	ADCP/WH-600	37° 02.6349′	75° 57.7698′	19/04/99 1802	12.8	12.5
	1	CT/SBE-26	36° 55.7239′	75° 59.8126′	9/09/99 1629	6.7	2
Autumn	1	CT/SBE-37	36° 55.7061′	75° 59.8110′	9/09/99 1630	6.1	5.8
	2	CT/SBE-37	36° 56.7707′	75° 59.2949′	9/09/99 1730	24.4	24.1
Deployment	3	CT/SBE-37	36° 57.6863′	75° 58.8147′	9/09/99 1500	22.0	2
	3	CT/SBE-37	36° 57.7708′	75° 59.1406′	9/09/99 1518	22.3	22
Sep–Nov	6	CT/SBE-26	37° 02.7366′	75° 57.1778′	9/08/99 1415	9.5	2
	6	CT/SBE-37	37° 02.5809′	75° 57.7663′	9/08/99 1356	12.2	11.9
1999	1	ADCP/WH-1200	36° 55.7061′	75° 59.8110′	9/09/99 1630	6.1	5.8
	2	ADCP/WH-600	36° 56.7707′	75° 59.2949′	9/09/99 1730	24.4	24.1
	3	ADCP/WH-300	36° 57.7708′	75° 59.1406′	9/09/99 1518	22.3	22
	4	ADCP/WH-600	36° 58.9817′	75° 58.8900′	9/08/99 1547	10.7	10.4
	5	S4	37° 00.4531′	75° 58.1754′	9/08/99 1458	6.4	3
	5	S4	37° 00.4531′	75° 58.1754′	9/09/99 1520	6.4	5
	6	ADCP/WH-600	37° 02.5809′	75° 57.7663′	9/08/99 1356	12.2	11.9

For the spring deployment the National Oceanic and Atmospheric Administration (NOAA)'s ship *Ferrel* was used to deploy five bottom-mounted RD Instruments "work-horse" ADCPs at M1, M2, M3, M4, and M6 (see Fig. 1) during April 19-22, 1999. Two Inter Ocean S4 current meters, one at mid-depth (~2.5 m from the surface) and one ~1 m above the bottom, were used for mooring 5. Another near-bottom S4 current meter was deployed at mooring 4. Each mooring was equipped with a Benthos acoustic pop-up buoy or an acoustic release. As a precaution, each mooring was also equipped with a Datasonics pinger to facilitate the recovery of the equipment. In addition to the moorings, six Seabird conductivity-temperature-depth (C/T) sensors were attached to the anchor chains of three navigation buoys, two on either side of the Chesapeake Channel and one in the North Channel. After a 75-day deployment, the recovery of the moored instruments was initiated on July 6. Of the six Benthos acoustic pop-up buoys/acoustic releases, only one deployed properly to provide a surface marker for recovery purposes. With the aid of a team of divers and the use of three boats over a period of a week, we were able to recover four ADCPs, three S4s, and one C/T sensor.

For the autumn deployment, five bottom mounted RDI workhorse ADCPs were deployed during September 7-9, 1999 at the entrance to the Chesapeake Bay (locations M1, M2, M3, M4, and M6) from the *Sea Search* (Fig. 1). Mid-water and near-bottom InterOcean S4 current meters again were used at mooring 5 and a near-bottom S4 was used at mooring 4. Each mooring was equipped with a Benthos acoustic pop-up buoy or an acoustic release, and a Datasonics pinger to facilitate the recovery of the equipment. Three Seabird C/T sensors were deployed next to the bottom-mounted ADCPs at moorings M1, M2, and M6. Three more C/Ts were attached near the surface to taut wires at moorings M1, M3, and M6. This distribution was dictated by logistical constraints related to ship traffic in the area. After a ~70-day deployment, the recovery of the moored instruments was initiated on November 9. Of the six Benthos acoustic pop-up buoys/acoustic releases, none deployed properly to provide a surface marker for recovery purposes. Once again, with the aid of a team of divers and the use of three boats over a period of two weeks, we were able to recover the five ADCPs, the three S4s, and all but one of the C/T sensors.

Values of daily river discharge for 1999 were obtained for the Susquehanna, Potomac and James from the United States Geologic Survey (USGS). Hourly sea level data were obtained from NOAA stations at the Chesapeake Bay Bridge Tunnel (CBBT Station #8638863), Kiptopeke (Station #8632200), Solomons (Station #8577330), and Baltimore (Station #8574680) (see Fig. 1 for station locations). These data were readily accessible through the National Ocean Service home page (http://www.co-ops.nos.noaa.gov). Hourly wind velocity data were obtained from stations at CBBT and Kiptopeke. All records of sea level, wind velocity, water temperature, velocity and salinity were low-passed with a 34-hr Lanczos filter to eliminate tidal variability. This work concentrates exclusively on the subtidal (i.e., the low-passed) signals.

4. Characterization of the observations

The spring-summer deployment was influenced by moderate river discharge (~2500 m^3/s) that was lower than the climatological mean and decreased slightly throughout the observation period. The buoyancy input during the autumn period was higher than the climatological mean because of the passage of tropical storm *Dennis* and Hurricane *Floyd.* The wind forcing and its influence on estuarine exchange for each deployment is described below.

a. Spring-summer deployment

During the first deployment, wind forcing was mostly northeasterly (NE) and southwesterly (SW) (Fig. 3a). Throughout the 75-day observation period there were 8 low-passed wind pulses that exceeded 5 m/s at CBBT: four NE wind pulses and four SW wind pulses. Northeasterly winds caused sea level to increase in the lower bay and southwesterly winds caused sea level to fall as depicted in the records at CBBT and the ADCP pressure sensors (Fig. 3b). Both wind components (easterly and northerly) showed a strong correlation with

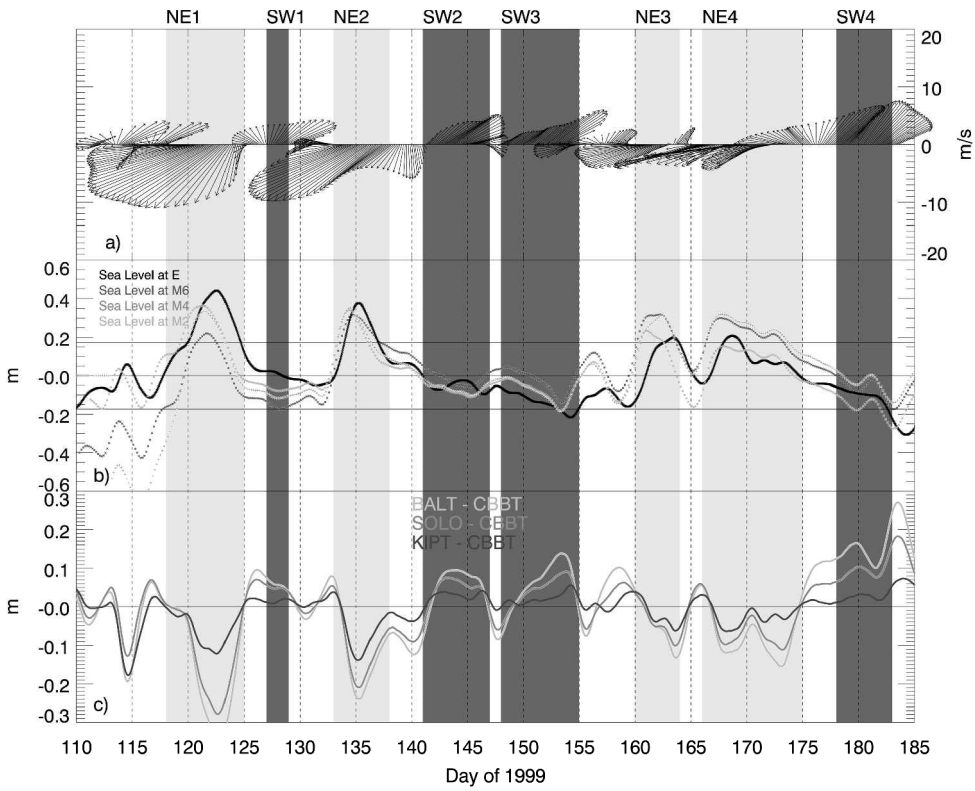

Figure 3. Time (GMT) series during the spring-summer deployment of wind velocity (a in meters per second), low-passed sea level (b in meters) at different locations in the lower bay, and differences in low-passed sea level (c in meters) between the Chesapeake Bay Bridge Tunnel station and three other locations across and along the bay. Wind velocities in (a) point in the direction toward which they blew. Horizontal lines (symmetric around zero) in (b) indicate the standard deviation of sea level during the period April-July of 1999. The sea level differences shown in (c) are representative of the sign of the sea level slopes, i.e., of the barotropic pressure gradient. The shaded bands represent the most energetic northeasterly or southwesterly wind pulses. Sea levels at M2, M4, and M6 were obtained with the ADCP pressure sensors.

sea level. The N-S wind component alone explained 75% of the sea level variance at CBBT (correlation coefficient of 0.87) with a zero lag and 64% of the sea level variance (correlation coefficient of 0.80) at mooring 2. The E-W component alone explained 59% of the sea level variance at CBBT and 64% of the variance at mooring 2, also with a zero lag. At mooring 2, the relationship between E-W wind component and sea level was better than at CBBT, and the correlation between N-S wind component and sea level was less than at CBBT because of the approximate E-W orientation of the mouth of the bay. In contrast, the CBBT location is at the transition between the N-S and E-W orientation of the bay. Inclusion of time lags improved these relationships by $<3\%$ and only for the E-W

component. A multiple regression that included both components of the wind explained 87% of the variance of the sea level at CBBT and 85% at mooring 2, a consistent response at both locations. In fact, the sea level variability of all the sensors was strongly coherent, which gave confidence in the sea level response of the lower Chesapeake Bay to wind forcing.

The increase of sea level in the lower bay associated with NE winds was not as dramatic in the upper bay (Baltimore or Solomons), which created a downward sea level slope from the mouth to the head, i.e., negative slopes (Fig. 3c). Also, the increase in sea level on the eastern side of the lower bay (Kiptopeke) related to NE winds was not as marked, which yielded a negative slope in the E-W direction. These gradients of sea level along and across the bay suggest that NE winds drove water from the coastal ocean toward the lower bay but also within the bay from north to south, thus creating a water bulge or a local high in dynamic topography against the southwestern corner of the bay, just off the mouth of the James River. The sea level differences also suggest that SW winds pushed water away from the southwestern corner of the Bay, thus creating a local low in dynamic topography by forcing water northward within the bay and seaward through the bay mouth. These hypotheses are further explored with the temperature-salinity properties and the velocity measurements.

Three salinity records were recovered from the instrumentation. Two records were from mooring 5 (near-bottom and mid-water) and one from mooring 6 (near-bottom). Both records at station 5, over the shallowest portion of the bay entrance, exhibited essentially the same temporal variability (Fig. 4a). Also, they both showed an average vertical difference in salinity of 2.04 ± 0.55 that exhibited weak fortnightly tidal modulation and indicated vertical stratification throughout the period of observation. The subtidal variability of salinity at both locations was strongly correlated (0.83 correlation coefficient) with subtidal sea level variability, thus salinity values at mooring 5 increased with NE winds and decreased with SW winds (Fig. 4b). Farther north, the near-bottom salinity at mooring 6 changed coherently with the variability observed at station 5. This fact suggests that subtidal salinity co-varied with subtidal sea level over the entire northern part of the bay entrance. Owing to the fact that there were no salinity records recovered from the southern half of the bay entrance then it is unknown whether such co-variability exists there. In the presence of conservative mixing a proxy for salinity can be derived from water temperature. The near-bottom temperature (de-trended and demeaned) at station 6 generally exhibited inverse correlation with salinity (Fig. 4c). The T-S relationship followed a nearly straight line of conservative mixing (Fig. 4d) with indication of some atmospheric heat gain. For the most part the T-S relationship indicated that low water temperatures corresponded with high salinities, i.e., they were related to coastal ocean waters. Waters of riverine origin were warmer than coastal ocean waters during this time of the year.

Near-bottom temperatures at moorings 4 (close to the middle of the entrance) and 2 (south) exhibited distinct variability from that at station 6 (to the north). In the Chesapeake Channel, near-bottom temperature initially increased with the onset of NE winds and

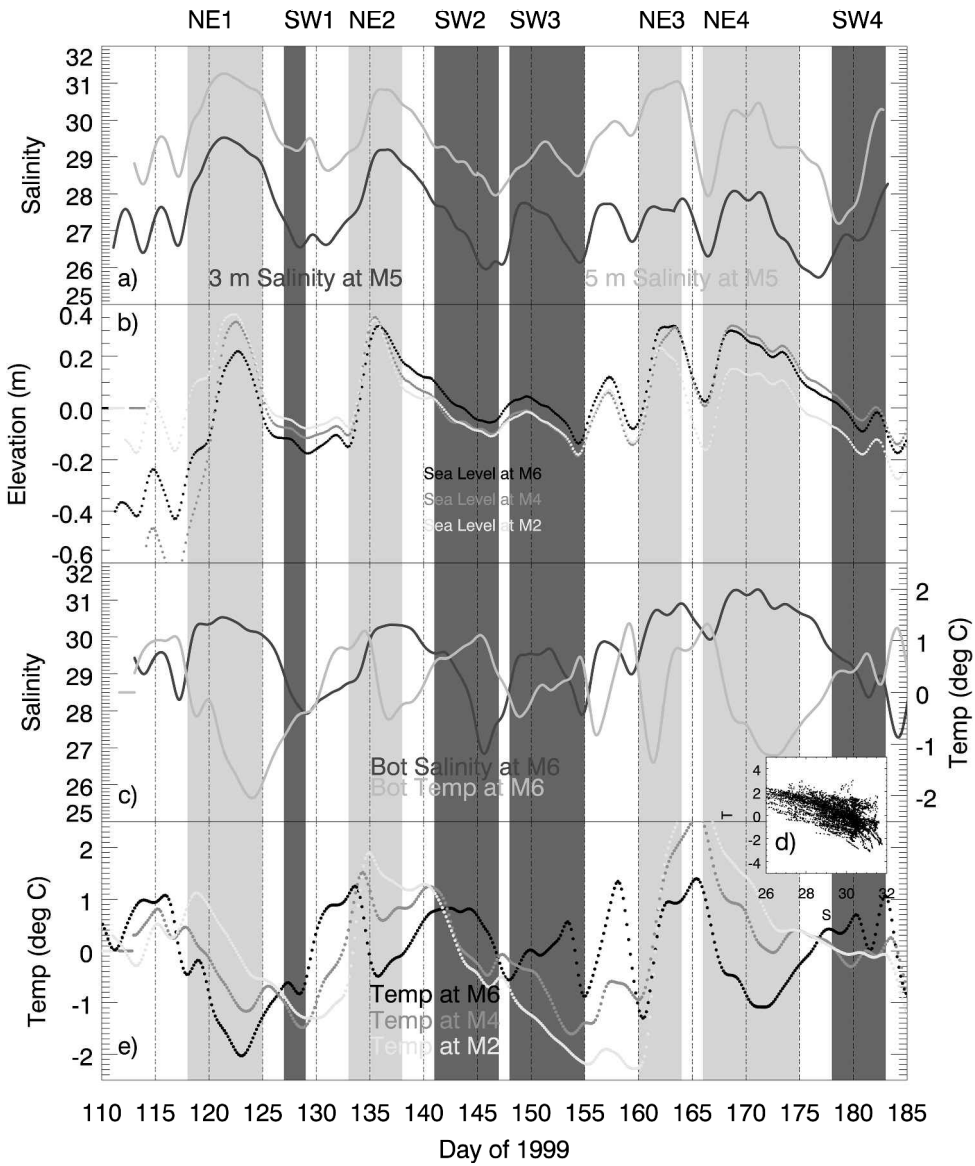

Figure 4. Time (GMT) series during the spring-summer deployment of low-passed salinity at 3 and 5 m deep at station M5 (a), low-passed sea level at different locations in the lower bay (b), the inverse relationship between detrended and de-meaned water temperature and salinity at station M6 (c) as also expressed by their T-S diagram (d), and bottom temperature (also de-trended and de-meaned) at different locations across the bay entrance. Note the different bottom temperature changes at each location produced by the same wind forcing.

increased sea level (Fig. 4e). Opposite variations occurred with SW winds. In general, positive anomalies in near-bottom temperatures at mooring 2 were associated with NE wind pulses and negative anomalies corresponded to SW wind pulses. All the records displayed on Figure 4 suggest that NE wind pulses drive near-bottom coastal ocean water into the Chesapeake Bay over the northern mouth of the bay (Stations 5 and 6) and near-bottom estuarine water out of the bay to the south. The transition between wind-induced inflow and outflow is inferred to occur around station 4 as suggested by its near-bottom temperature variations, which appeared between stations 2 and 6 (Fig. 4e).

Subtidal flow profiles at each station are now used to further describe the responses produced by NE and SW winds. The four NE wind pulses that occurred during the spring-summer period generated similar patterns of exchange flow. A depth-independent downwind flow, as expected from theory, appeared over the northern, shallow part of the entrance (Fig. 5). However, the dramatically different response over the southern portion of the entrance was unexpected. There, the flow was strongest and to the left of the wind, i.e., NE winds drove net outflow throughout the water column. Transverse differences in the vertical structure of the outflow were present from the southernmost and shallow area off Cape Henry to the deepest part of the entrance in Chesapeake Channel. Within the southernmost sector of the bay entrance, off Cape Henry, the outflow was depth-independent but in Chesapeake Channel it veered clockwise with increasing depth, reminiscent of an Ekman spiral. Within this channel, the flow tended to align toward the downwind direction as distance from the surface increased. A possible reason for this clockwise veering with increased depth is discussed in Section 5.

The four southwesterly wind pulses also induced consistent flow patterns at the bay entrance (Fig. 6). These winds produced exchange configurations that preferentially took place in the vertical plane, in contrast to the exchanges in the horizontal plane resulting from NE winds. Southwesterly winds drove near-surface water out of the bay across the entire entrance region. Over the shallow areas in the middle of the bay entrance, outflow was nearly depth-independent. A compensatory inflow, which was stronger than under no-wind conditions or any other wind conditions, was present near the bottom of the channels (Chesapeake and North). This scenario is consistent with higher spatial resolution observations taken during weaker wind situations (Valle-Levinson *et al.,* 1998) (e.g. Fig. 2). Nonetheless, the observations in the spring-summer period indicate that the strongest near-bottom inflows in the channels of the bay entrance are driven by SW winds. Thus, it seems that SW winds tend to drive the most effective exchange of water between the lower Chesapeake Bay and the adjacent coastal waters. It is important to note that a depth-independent inflow rapidly ensued in the channels after the SW wind pulses relaxed.

The exchange patterns described for NE and SW winds were indeed dominated by wind forcing as they remained qualitatively the same after subtracting the mean flows (averaged over the entire deployment), which are shown at the end of the following subsection. Also worth noting is the paradox demonstrated by the asymmetrical response of the currents to

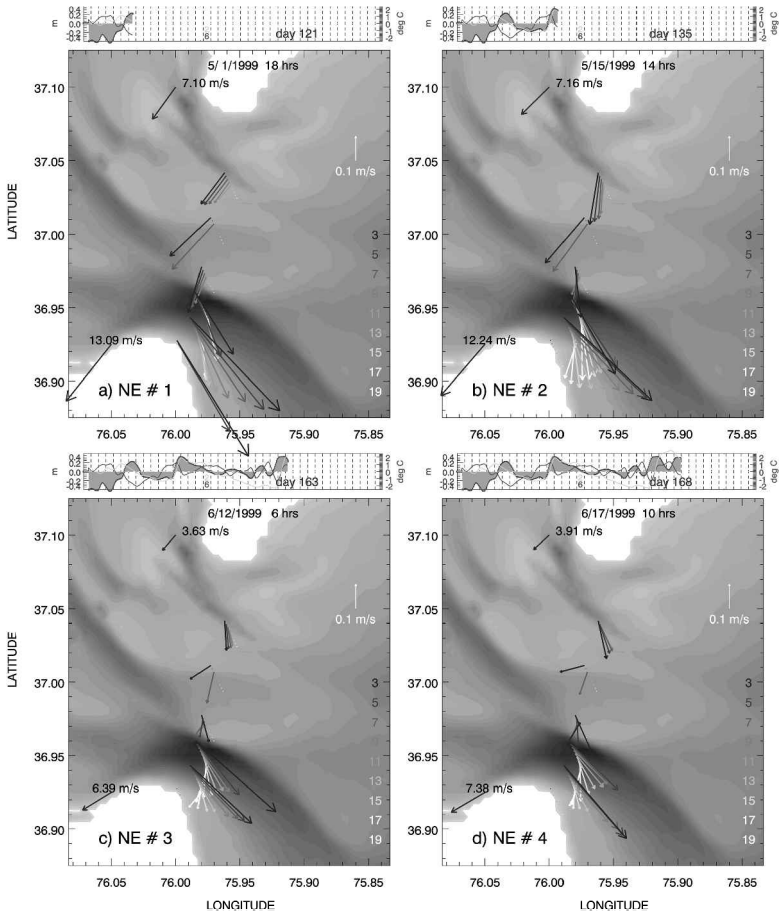

Figure 5. Subtidal flows (represented by vectors) recorded at different depths under the influence of the four northeasterly wind pulses during the spring-summer deployment. The vectors are plotted on the bathymetry of the lower Chesapeake Bay as in Figure 1. The upper segment of each panel illustrates the subtidal sea level (shaded), and the bottom temperature at the northern end (mooring 6) and southern end (mooring 2) of the entrance to the bay to illustrate the different responses to the same wind. Wind vectors at CBBT and Kiptopeke are labelled with their magnitude just to the west of Cape Henry and Fishermans Island, respectively. This is not the exact location of wind measurements but serves to illustrate the spatial coherence of the two sites. Flow arrows are plotted at a slight shift of latitude and longitude to appreciate their variability throughout the water column. The depth associated with each vector is shown by the number on the right of each panel and its scale is presented on the upper right portion. All times are GMT.

the direction of wind forcing in contrast with the symmetrical response of the sea level. This paradox underscores the need for caution when describing exchange flows based on sea level observations alone.

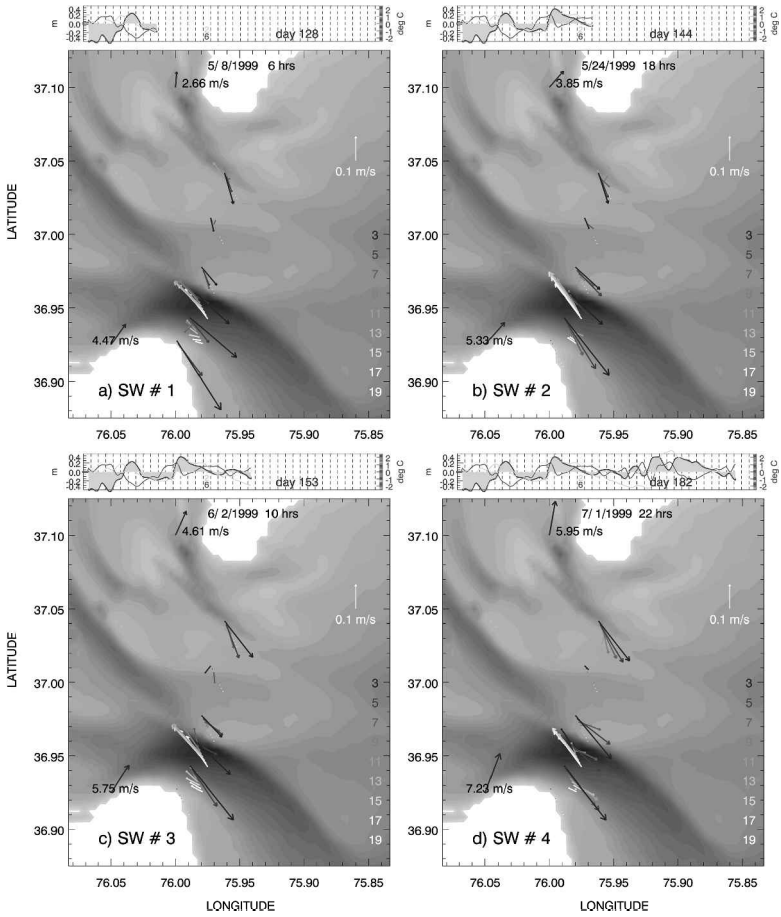

Figure 6. Same as Figure 5 but for southwesterly wind pulses.

b. Autumn deployment

During the autumn deployment, winds were predominantly from the NW and SW (Fig. 7a). In this ~70-day period of observations four northwesterly wind pulses caused consistent sea level slopes, salinity and flow variations. Three southwesterly wind pulses produced similar responses to those observed in the spring-summer deployment. In addition, the passage of Hurricane *Floyd* over the study area caused winds that changed rapidly from the northeast to the northwest and a response comparable to that induced by NE winds. The wind and buoyancy pulses related to *Floyd* merit special attention and are addressed in a separate study (Valle-Levinson *et al.,* 2000). Only the generalities of these pulses are mentioned here.

During the entire autumn deployment wind pulses were more variable than in the first deployment and also of shorter duration. This was reflected by rapid variations of subtidal

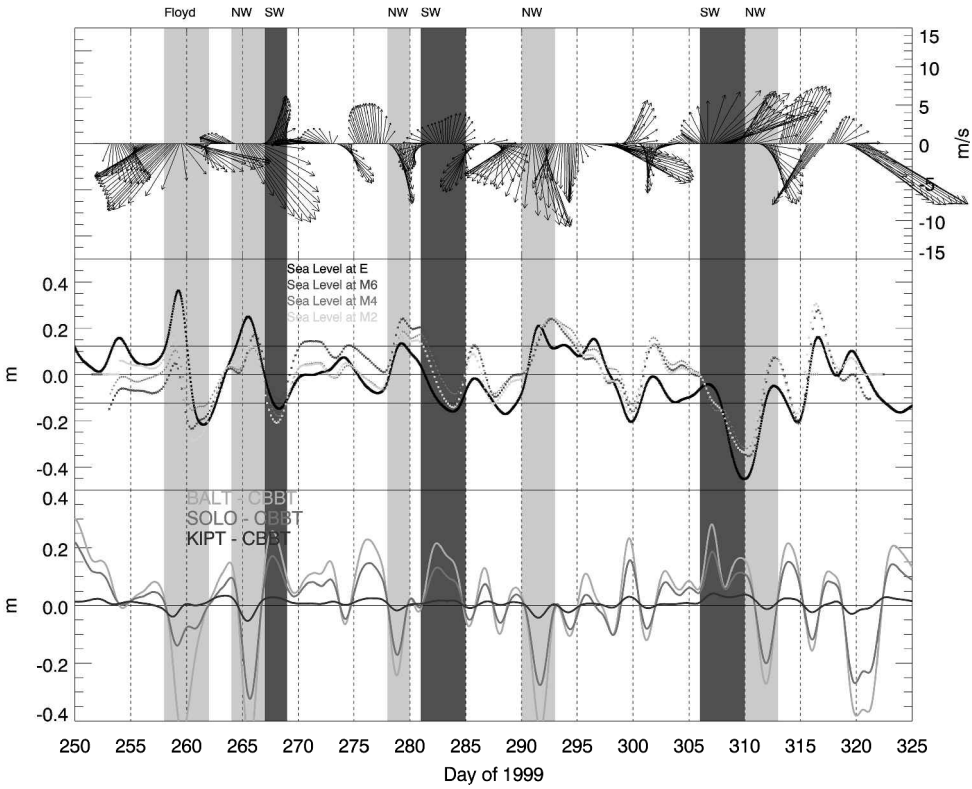

Figure 7. Same as Figure 3 but for the autumn deployment. Four NW wind pulses, 3 SW wind pulses, and forcing from Hurricane *Floyd* are identified as the extreme events.

sea level (Fig. 7b) that had a decorrelation time scale of ~1 day in contrast to the spring-summer deployment that exhibited a decorrelation time scale of ~2 days. The largest sea level increases during the autumn deployment were related to NW winds while the largest sea level drops were again associated with SW winds. An exception to the patterns identified for NW and SW winds occurred around September 15-16 (days 258-259) with the passage of Hurricane *Floyd* over the area with rapidly changing strong winds that caused a swift increase and ensuing decrease of sea level in less than 2 days. The sea level slopes observed throughout the autumn deployment were consistent with those observed during the spring-summer period. Southwesterly winds caused sea level to slope up toward the north and east as demonstrated by the positive differences between CBBT and each of the other three locations (Fig. 7c). Northwesterly winds caused negative slopes between CBBT and all of the other three locations and piled up water on the SW corner of the bay, analogously to NE winds (days 265, 279, 291 and 311). The influence of these significant wind pulses on subtidal salinity and flow fields is explored below.

Subtidal salinities were well correlated with sea level (around 0.5) and wind forcing

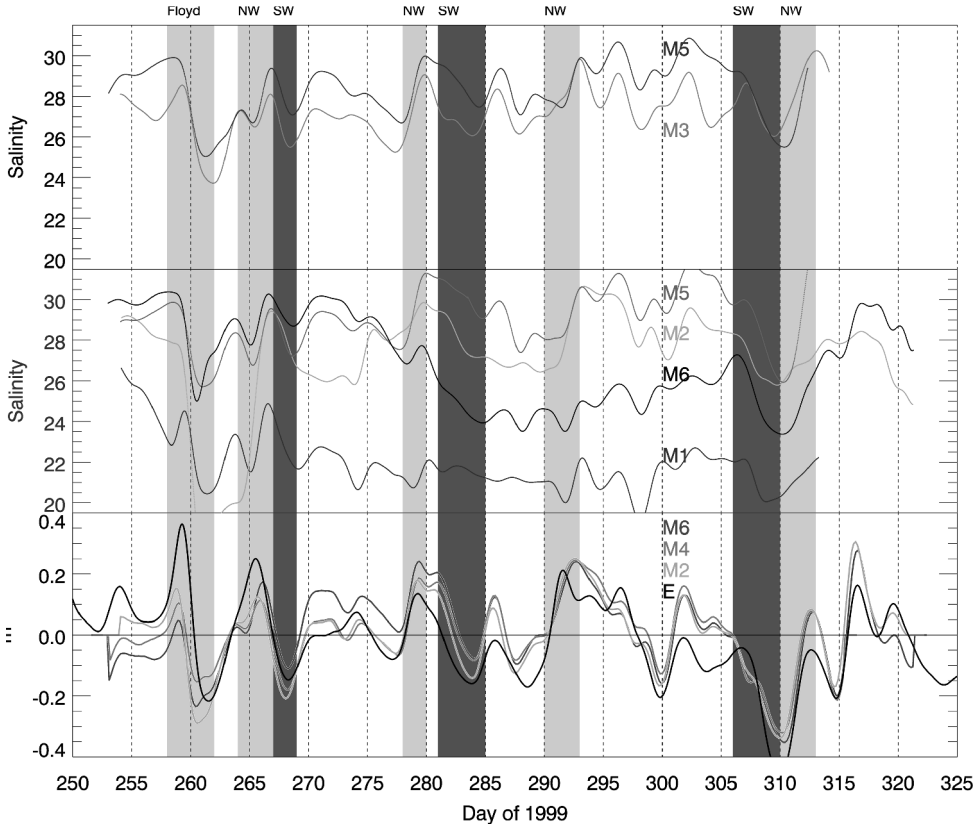

Figure 8. Time (GMT) series during the autumn deployment of low-passed near-surface salinity at stations M3 and M5 (a), low-passed near-bottom salinity at stations M1, M2, M5 and M6 (b) (the signal at M3 was fouled after *Floyd*), and low-passed sea level at different locations in the lower bay (c).

(Fig. 8). In general, the salinity variability was coherent between each location where a record was recovered (two near-surface and four near-bottom records) during the strongest wind events (shaded on Figs. 7 and 8). The four northwesterly wind pulses caused a local salinity drop of short duration at the onset of NW winds, but this was quickly followed by an overall salinity increase. Analogously, the three southwesterly wind pulses caused coherent salinity drops throughout the lower bay. Three other salinity decreases were observed: one related to a brief SW wind pulse on day 287, another caused by a WNW wind pulse on day 298, and the largest drop on days 259-260 related to Hurricane *Floyd*. In this pulse, salinity dropped coherently across the bay and also in the entire water column by as much as 8 units in 1 day (Station 2 of Fig. 8). Interestingly, the freshwater signal appeared first over the northern part of the entrance, at station 6, although the reason for this response is unclear. As expected, the surface signal lead the bottom due to its buoyant

nature. Salinity began to decrease only a few hours after the passage of the hurricane and rebounded soon after the wind and buoyancy pulse relaxed, on September 19 (day 262), even a bit earlier on Station 6. Salinity values decreased once more throughout the bay on day 264 owing to another NW wind pulse. The whole bay entrance returned to pre-hurricane conditions approximately 10 days after the storm (on day 268). Even though the autumn period of observations was influenced by tropical systems that dumped large amounts of fresh water in the area, the water column remained less stratified than during the spring-summer period.

The subtidal flow in the lower bay during the three SW wind pulses was similar to the pattern observed during the first deployment: bi-directional flow in Chesapeake and North Channels and seaward flow elsewhere. Near-bottom inflow associated with the bi-directional flows, however, was not as well developed in the autumn as it was in the spring-summer (Fig. 9). This can be attributed to weaker water column stratification that allowed a more efficient vertical transfer of horizontal momentum by the wind throughout the water column. The relaxation of SW winds was followed by net inflows throughout the water column.

This period of observation also allowed the characterization of the wind-induced flow produced by NW winds. As suggested by the salinity data, NW pulses caused two types of responses, one when the CBBT wind was >12 m/s and one when it was ≤ 12 m/s. Strong NW pulses caused net outflow everywhere across the mouth and throughout the water column (Figs. 10a, 10c). This response is analogous to that produced by NE winds in the sense that net outflow developed in Chesapeake Channel. Also reminiscent of the response to NE winds were the clockwise veering with increasing depth in Chesapeake Channel and the downwind flow over the shallower portions of the entrance. The two strong NW wind pulses caused an initial salinity drop and then, as the wind weakened, net inflow developed near the bottom with a subsequent salinity increase. Relatively weaker NW pulses drove near-surface outflow everywhere and near-bottom inflow or southward flow across the mouth, hence the corresponding salinity increase (Figs. 10b, 10d). The passage of *Floyd* caused a flow structure that was consistent with a large flushing of fresh water out of the bay throughout the water column (Fig. 11a), similar to the response to strong NW winds. The subtidal flow was directed seaward everywhere at the bay entrance with near-surface values of up to 0.5 m/s. The strong outflow can be attributed, in addition to wind stress, to the strong barotropic pressure gradient caused by freshwater discharge. The barotropic pressure gradient apparently overcame the tendency of the baroclinic pressure gradient to cause inflow near the bottom. In other words, the initial response of the estuary to river discharge was barotropic, not baroclinic. After the wind and buoyancy pulse relaxed, a depth-independent subtidal inflow was established on day 262 (Fig. 11b).

The mean flows for the spring-summer and autumn periods of observation (Fig. 12) featured typical magnitudes of less than 0.10 m/s and a spatial structure that was consistent with the "Non-Southwesterly Wind" scenario depicted in Figure 2. Gravitational circulation was evident in the channels, whereas a depth-independent outflow was present off the

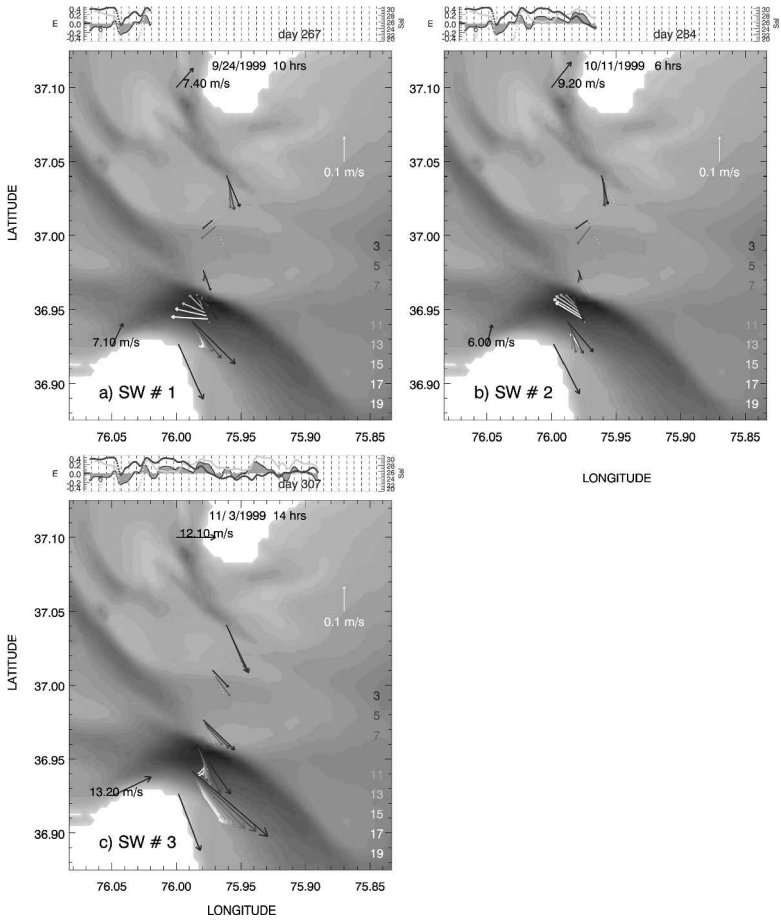

Figure 9. Same as Figure 6 but for the autumn deployment. The upper panels now show bottom salinities (instead of temperatures) at moorings 2 and 6.

southern cape (Cape Henry), and tendencies for recirculation appeared between the channels. The similarity portrayed by the mean flows of both periods was remarkable and postulates the expected structure of the mean flows under no-wind conditions, i.e., the "Relaxation" conditions.

5. Outflow related to northerly winds and clockwise veering with depth

The development of net outflow over the southern part of the entrance with NE and NW winds and the clockwise veering with increasing depth of this flow are explored in this section. Using a streamwise coordinate system (e.g. Kalkwijk and R. Booij, 1986; Thorne and Hey, 1979) the momentum balance normal to the streamwise flow, which most likely

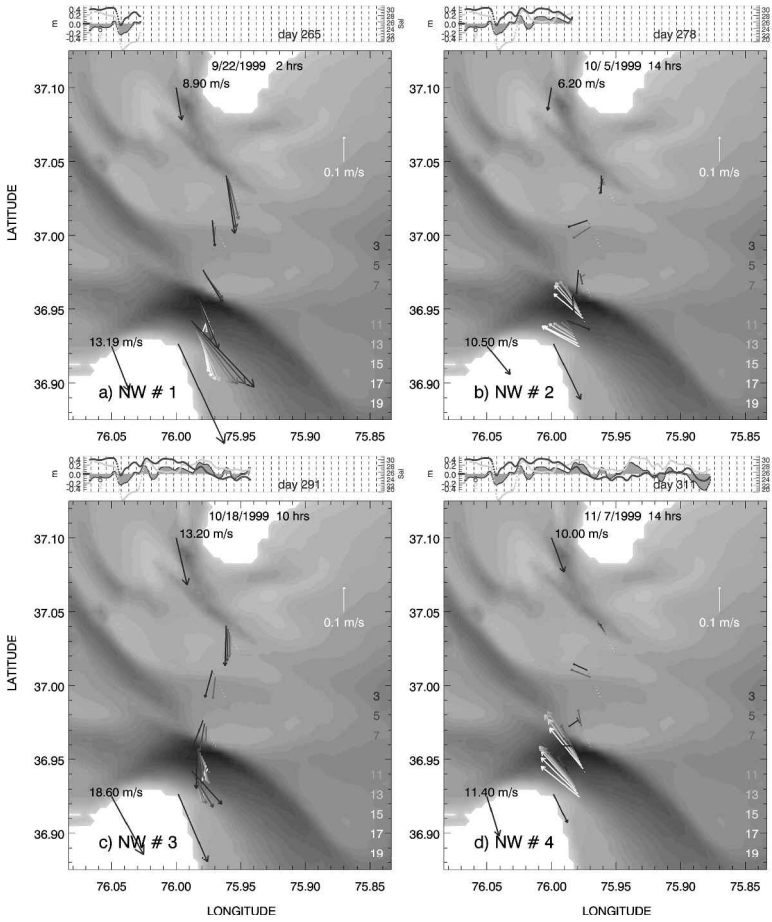

Figure 10. Same as Figure 9 but for Northwesterly winds.

produced the observed flow in the vicinity of Cape Henry, is among centripetal, Coriolis, and pressure gradient accelerations, or:

$$\frac{U_s^2}{R} + fU_s = -g\frac{\partial \eta}{\partial n}, \tag{1}$$

where U_s is the streamwise flow, perpendicular to the n direction, positive seaward; f, g, R, and η, are the Coriolis parameter ($8.8 \times 10^{-5}\ s^{-1}$), the acceleration due to gravity ($9.8\ m/s^2$), the radius of curvature (5 km around Cape Henry) and surface elevation, respectively. The nonlinear terms have been represented by the centripetal acceleration U_s^2/R as in Doyle and Wilson (1978). The accelerations induced by the wind stress are inversely related to the water column depth and therefore exert a lesser influence (of order $10^{-6}\ m/s^2$) on the subtidal flow in the deep Chesapeake Channel. Bottom stresses related to

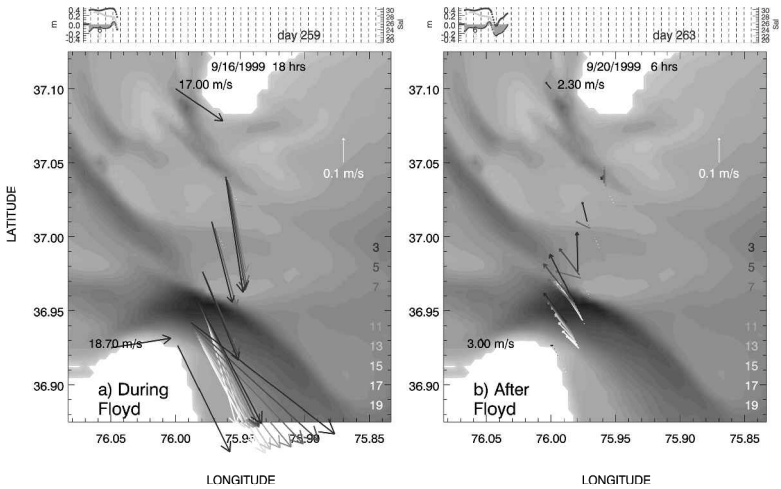

Figure 11. Same as Figures 9 and 10 but during and after the passage of Hurricane *Floyd.*

the flow in the normal direction are even weaker and hence they have been omitted from (1). Note that (1) is second order on U_s and can be solved algebraically for different values of R and $\partial\eta/\partial n$ for a given f and g. The positive of the two values of U_s (Fig. 13a) approaches the geostrophic value as R increases; i.e., as centripetal accelerations decrease. The solution also shows that for any given sea level slope the greatest change of U_s occurs

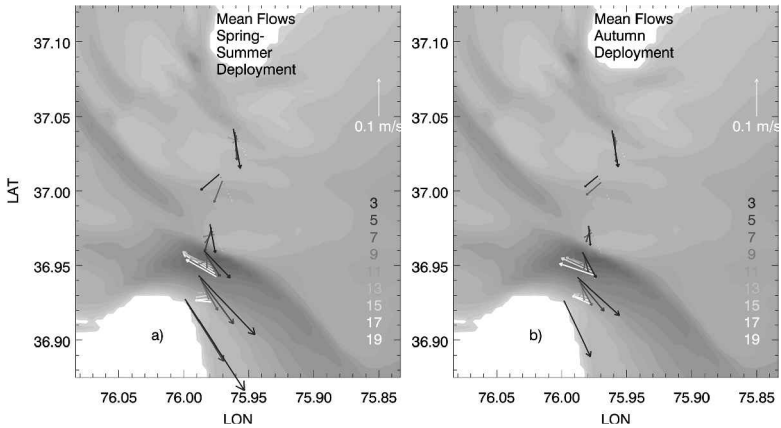

Figure 12. Mean flows (represented by vectors) recorded at different depths over the entire (a) spring-summer and (b) autumn deployments. The vectors are plotted on the bathymetry of the lower Chesapeake Bay as in Figure 1. Flow arrows are plotted at a slight shift of latitude and longitude to appreciate their variability throughout the water column. The depth associated with each vector is shown by the number on the right of each panel and its scale is presented on the upper right portion.

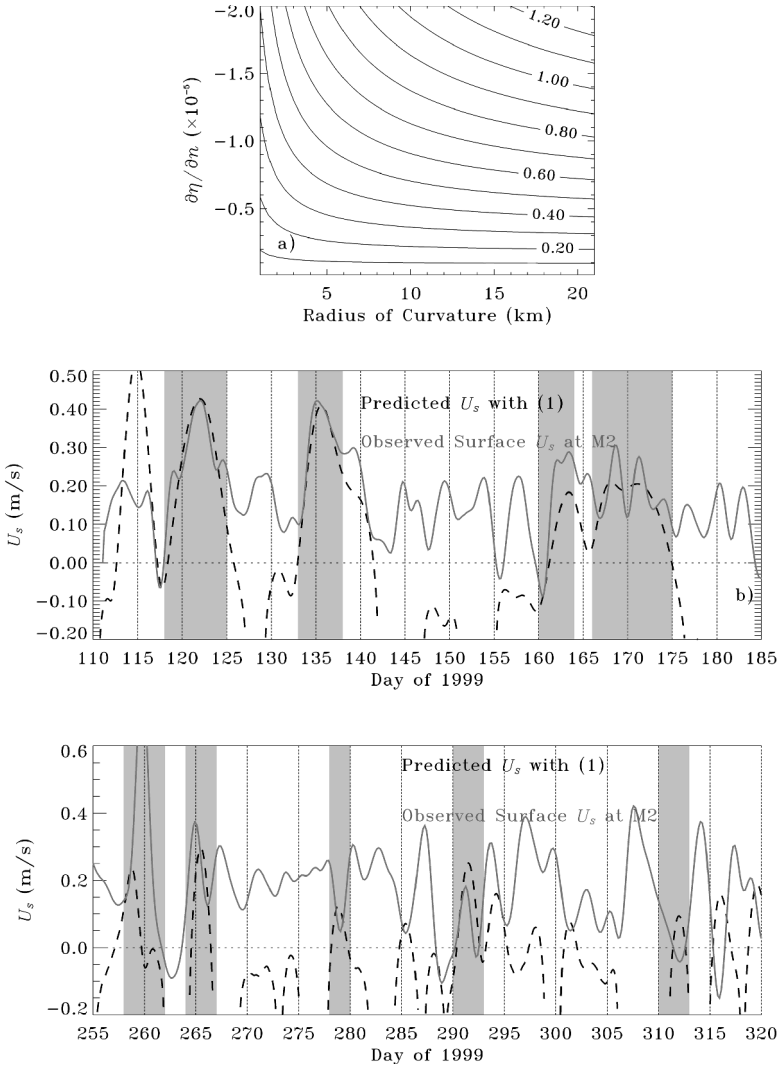

Figure 13. (a) Predicted surface flows U_s from Eq. (1) for different radius of curvature and sea level slopes. (b) Comparison of predicted surface flows U_s from Eq. (1) (dashed line) to observed surface flows at M2 in the Chesapeake Channel (continuous line) during the spring-summer deployment. The shaded periods denote northeasterly wind pulses, which are the only periods when Eq. (1) is assumed to apply. (c) Comparison of predicted surface flows U_s from Eq. (1) (dashed line) to observed surface flows at station 2 in the Chesapeake Channel (continuous line) during the autumn deployment. The shaded periods denote northeasterly and northwesterly wind pulses, which are the only periods when Eq. (1) is assumed to apply. Note that the best matches developed around days 265 and 292, when NW winds >12 m/s.

at small values of R (<5000 m). Taking the observed subtidal sea level slope between CBBT and Kiptopeke and an R around Cape Henry of 5 km, then the values of U_s predicted by (1) agree very well with the observed near-surface values in Chesapeake Channel during NE wind pulses (periods marked on Fig. 13b). This agreement strongly suggests that the dynamics of the NE wind-induced outflow are closely represented by (1). Inclusion of observed wind stress in (1) caused negligible changes to U_s.

During the autumn deployment the similarity between observations and values predicted by (1) holds best only during strong (>12 m/s) NW winds (days 265 and 292 in Fig. 13c), which is when the subtidal flow patterns most resemble those produced by NE winds (Figs. 10a and 10c). The predicted U_s is also close to the observed flow during the NE winds of *Floyd* (day 258). The significantly larger observed flow by day 260 is most likely due to the strong pulse of fresh water leaving the bay as evidenced by the salinity records (Fig. 8). Furthermore, it is likely that the flow established by the wind-induced (NE and NW) sea level slopes is not in geostrophic balance, otherwise it would be in the same direction throughout the water column. The magnitude predicted by the geostrophic approximation overestimates the observations by ~50%. Hence, the centripetal accelerations tend to reduce the magnitude of the geostrophic flow.

The clockwise veering with increasing depth exhibited by the outflow in the Chesapeake Channel may be explained by continuing to assume that the dynamics associated with the outflow are mostly governed by (1). As U_s tends to lose strength with increasing depth R has to decrease in order for (1) to be maintained because f, g and $\partial\eta/\partial n$ do not change with depth. The effective radius of curvature decreases parabolically as dictated by (1) in such a way that R becomes less than half the surface value by mid-depth and ~4 times smaller near the bottom relative to the surface. The outflow veering thus develops in the direction of the centripetal acceleration as the radius of curvature becomes smaller, i.e., toward the bend. Paradoxically, in this case the flow below the surface tends to align more with the direction of the wind than the flow at the surface but does not appear to be driven directly by wind stress. It is important to note that the clockwise veering is not associated with a bottom Ekman spiral (friction balanced by Coriolis accelerations), otherwise the net flow would veer in the opposite direction to that observed, i.e., counterclockwise.

6. Discussion

Analysis of moored ADCP and CT data during spring-summer and autumn deployments revealed responses of the lower Chesapeake Bay to wind forcing, which are presented schematically in Figure 14. A relaxation scenario was identified, consistent with the non-southwesterly wind scenario proposed by Valle-Levinson *et al.* (1998), in which gravitational circulation was observed in the channels and a recirculation over Six-Meters Shoal (Fig. 14a). This exchange scenario corresponds to the mean flow estimated over the length of each deployment (Fig. 12), i.e., it is associated with the density-induced flow. Northeasterly winds caused sea level to slope downward from the mouth to the head of the estuary and from the west to the east. Water piled-up on the southwestern corner of the

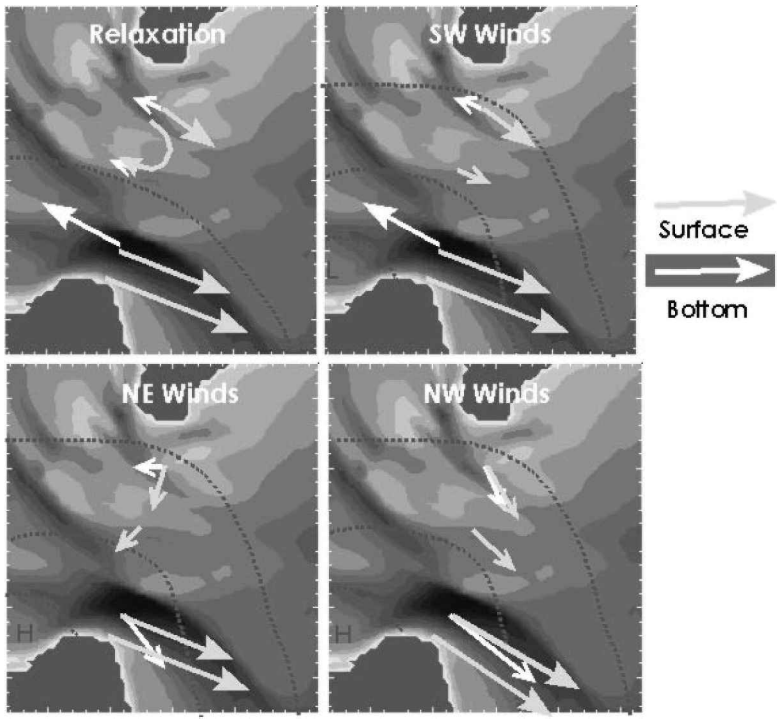

Figure 14. Water exchange patterns suggested by the observations obtained in this study. The dotted lines represent dynamic topography as suggested by sea level measurements.

Chesapeake Bay owing to wind-driven transport from the ocean and from inside the bay itself. The inflow of water produced by northeasterly winds was expected. However, the strong outflow observed around Cape Henry was completely unexpected as it moved to the left of the wind direction (Fig. 14b). The response of the subtidal flow to the four northeasterly wind pulses observed during the spring-summer period was essentially the same, which gave more credence to the unexpected flow pattern. The piling of water up against the southwestern corner of the bay represented a pressure head that drove water out of the bay, most likely under the influence of Coriolis and centripetal accelerations, over the southern portion of the entrance to the bay (off Cape Henry). This outflow veered clockwise with increasing depth, reminiscent of a surface Ekman spiral although dynamically different. The flow over the northern half of the entrance to the bay moved with the wind, i.e., into the estuary.

Southwesterly winds caused sea level to slope upward from the mouth to the head of the estuary and from the west to the east. A low in dynamic topography appeared on the southwestern corner of the Chesapeake Bay owing to wind-driven transport toward the ocean and toward the upper bay. Wind-induced surface flow was out of the bay across the entire entrance (Fig. 14c). Outflow also appeared throughout the water column over the

shallow areas between the channels. A compensatory inflow developed near the bottom in the Chesapeake Channel. This compensatory inflow was markedly weaker in the autumn than in the spring-summer due to stratification differences. This scenario is consistent with the flow patterns observed with shipboard measurements. Southwesterly winds then tend to enhance bi-directional flow in the channels and to produce outflow over the relatively shallow portion between the channels.

Noteworthy during the autumn deployment were the northwesterly pulses and the passage of Hurricane *Floyd* over the study area on September 16, 1999. Northwesterly winds produced a similar response in the Chesapeake Channel as that produced by northeasterly winds, i.e., flow out of the estuary (Fig. 14d). Over the northern, shallower half of the bay entrance the northwesterly wind-induced flow also was out of the estuary throughout the water column. Therefore, northwesterly winds were identified as the most efficient in flushing the water out of the estuary. The passage of Hurricane *Floyd* caused a large flushing of fresh water out of the bay throughout the water column. Subtidal salinities dropped by as much as 8 units in 1 day. Salinity began to decrease only a few hours after the passage of the hurricane, which dumped rain in excess of 300 mm. Salinity values returned to before-hurricane conditions approximately 10 days after the storm. The most relevant result of this forcing was the flushing of freshwater throughout the water column due to the strong barotropic pressure gradient caused by freshwater discharge. This apparently overcame the tendency of the baroclinic pressure gradient to cause inflow near the bottom. In other words, the initial response of the estuary to river discharge was barotropic, not baroclinic.

The present study reveals that the wind-induced current pattern at the mouth of Chesapeake Bay is consistent with findings from Delaware Bay (Wong and Moses-Hall, 1998a,b) in that it displays appreciable transverse variability, with the currents over the shoals exhibiting very different patterns from those in the channel. Similar to the Delaware Bay, the surface and bottom currents over the shoals flow largely in the same direction, while those over the channel exhibit significant variation with depth depending on the wind conditions. Furthermore, the present study also reveals features in the estuary-shelf exchange patterns which have not been well-documented in other systems. While the currents over the channel flow roughly in the longitudinal direction, there may be substantial depth-dependent veering to the left of the wind or a flow reversal with depth depending on the direction of the prevailing winds. Moreover, the direction of the current over the shoal is strongly controlled by the wind direction. As a result, the flow over the shoals may be dominated by a transverse current rather than current in the longitudinal direction.

The present study indicates that the overall effect of wind on the exchange of material between an estuary and the shelf cannot be assessed on the basis of sea level measurements alone, as the barotropic inflow (outflow) associated with coastal set-up (set-down) in no way reflects the observed exchange pattern. This study also shows the importance of the interaction between local wind forcing and bathymetry in producing the complex estuary-

shelf exchange pattern. The exchange processes between the estuary and the shelf cannot be properly examined without resolving the transverse variability of the exchange flows. Both of these findings, the inadequacy of sea level measurements to infer exchange flows and the need to elucidate transverse variability, contribute to our understanding on wind-induced exchange in estuarine and coastal waters.

7. Summary

The innovative findings of this study of wind-induced exchange may be summarized as follows. (1) Northeasterly winds tend to cause depth-independent volume inflow only over the northern half of the entrance to the estuary. A strong outflow that veers clockwise with increasing depth, but without reversing direction, develops around the southern cape (Cape Henry) in response to those northeasterlies. (2) Northwesterly winds are the most efficient in flushing estuarine waters out at every depth. This is mostly due to the orientation of the Chesapeake Bay because the wind drives water out over the shallow and northern regions of the entrance, and the wind-induced pressure gradient drives water out over the deeper and southern portions. (3) A strong pulse of fresh water like that produced by pluvial precipitation from Hurricane *Floyd* generates a depth-independent outflow across the entire estuary. This response develops only within a couple of days after the heavy rains. The estuary recovers its pre-event salinity after approximately ten days of the decrease. In general, this study suggests that in order to characterize exchange flows at the mouth of a coastal plain estuary the transverse variability of the flows needs to be elucidated and that sea level measurements alone will yield insufficient information.

Acknowledgment. This work is funded by the U.S. National Science Foundation under grant OCE-9812206 to AVL and KTB, and OCE-9810649 to KCW. Successful deployments and recoveries were accomplished with the help of many people and several vessels. The logistic support of R. Moody, R. C. Kidd, and A. Sundberg is greatly appreciated as well as the help of C. Reyes, A. Sepulveda, K. Holderied, R. Sanay, and M. Caceres. The NOAA/NOS field operations team provided invaluable support. Thanks to the crew of the NOAA ship *Ferrel,* under the able command of LCDR Paul Moen, for their very professional support. Also, the crew of the *Sea Search* and the divers from Chesapeake Divers were crucial in the recovery efforts.

REFERENCES

Browne, D. R. and C. W. Fisher. 1988. Tide and tidal currents in the Chesapeake Bay. NOAA Tech. Rep. NOS OMA 3, U.S. Dept. of Commerce, Rockville, MD, 143 pp.

Chuang, W.-S. and W. C. Boicourt. 1989. Resonant seiche motion in the Chesapeake Bay. J. Geophys. Res., *94,* 2105–2110.

Csanady, G. T. 1973. Wind-induced barotropic motion in long lakes. J. Phys. Oceanogr., *3,* 429–438.

Doyle, B. E. and R. E. Wilson. 1978. Lateral dynamic balance in the Sandy Hook to Rockaway Point transect. Estuar. Coast. Mar. Sci., *6,* 165–174.

Elliott, A. J. 1978. Observation of the meteorologically induced circulation in the Potomac estuary. Estuar. Coast. Mar. Sci., *6,* 285–299.

Fischer, H. B. 1976. Mixing and dispersion in estuaries. Ann. Rev. Fluid Mech., *8,* 107–133.

Friedrichs, C. T. and J. M. Hamrick. 1996. Effects of channel geometry on cross sectional variations in along channel velocity in partially stratified estuaries, *in* Buoyancy Effects on Coastal and Estuarine Dynamics, Coastal and Estuarine Studies, American Geophysical Union, *53,* 283–300.

Geyer, W.R. 1997. Influence of wind dynamics and flushing of shallow estuaries. Estuar. Coast. Shelf Sci., *44,* 713–722.

Glorioso, P.D. and A.M. Davies. 1995. The influence of eddy viscosity formulation, bottom topography, and wind wave effects upon the circulation of a shallow bay. J. Phys. Oceanogr., *25,* 1243–1264.

Goodrich, D.M. 1988. On meteorologically induced flushing in three U.S. east coast estuaries. Estuar. Coast. Shelf Sci., *26,* 11–121.

Goordich, D.M., W.C. Boicourt, P. Hamilton and D.W. Pritchard. 1987. Wind-induced destratification in Chesapeake Bay. J. Phys. Oceanogr., *17,* 2232–2240.

Hearn, C.J., J.R. Hunter and M.L. Heron. 1987. The effects of a deep channel on the wind-induced flushing of a shallow bay or harbor. J. Geophys. Res., *92,* 3913–3924.

Hunter, J.R. and C.J. Hearn. 1987. Lateral and vertical variations in the wind-driven circulation in long, shallow lakes. J. Geophys. Res., *92,* 13,106–13,114.

Kalkwijk, J.P.T. and R. Booij. 1986. Adaptation of secondary flow in nearly-horizontal flow. J. Hydraul. Res., *24,* 19–37.

Kjerfve, B., J.E. Greer and R.L. Crout. 1978. Low-frequency response of estuarine sea level to non-local forcing, *in* Estuarine Interactions, M.L. Wiley, ed., Academic Press, 497–513.

Kjerfve, B. and B.A. Knoppers. 1991. Tidal choking in a coastal lagoon, *in* Tidal Hydrodynamics, B. Parker, ed., John Wiley, 169–181.

Noble, M.A., W.W. Schroeder, W.J. Wiseman Jr., H.F. Ryan and G. Gelfenbaum. 1996. Subtidal circulation patterns in a shallow, highly stratified estuary: Mobile Bay, Alabama. J. Geophys. Res., *101,* 25,689–25,703.

Paraso, M.C. and A. Valle-Levinson. 1996. Meteorological influences on sea level and water temperature in the lower Chesapeake Bay: 1992. Estuaries, *19,* 548–561.

Pollak, M.J. 1960. Wind set-up and shear-stress coefficient in Chesapeake Bay. J. Geophys. Res., *65,* 3383–3389.

Schroeder, W.W. and W.J. Wiseman Jr. 1986. Low-frequency shelf-estuarine exchange process in Mobile Bay and other estuarine systems on the northern Gulf of Mexico, *in* Estuarine Variability, D.A. Wolfe, ed., Academic Press, 355–367.

Signell, R.P., R.C. Beardsley, H.C. Grabor and A. Capotondi. 1990. Effect of wave-current interaction on wind-driven circulation in narrow, shallow embayments. J. Geophys. Res., *95,* 9671–9678.

Smith, N.P. 1977. Meteorological and tidal exchange between Corpus Christi Bay, Texas and the northwestern Gulf of Mexico. Estuar. Coast. Mar. Sci., *5,* 511–520.

—— 1978. Long-period, estuarine-shelf exchange in response to meteorological forcing, *in* Hydrodynamics of Estuaries and Fjords, J.C.J. Nichoul, ed., Elsevier, 147–159.

Thorne, C.R. and R.D. Hey. 1979. Direct measurements of secondary currents at a river inflexion point. Nature, *280,* 226–228.

Valle-Levinson, A. 1995. Observations of barotropic and baroclinic exchanges in the lower Chesapeake Bay. Cont. Shelf Res., *15,* 1631–1647.

Valle-Levinson, A. and K.M.M. Lwiza. 1998. Observations on the influence of downwelling winds on the Chesapeake Bay outflow, *in* Physics of Estuaries and Coastal Seas, J. Dronkers and M. Scheffers, eds., A.A. Balkema Rotterdam, 247–256.

Valle-Levinson, A., C. Li, T. Royer and L. Atkinson. 1998. Flow patterns at the Chesapeake Bay entrance. Cont. Shelf Res., *18,* 1157–1177.

Valle-Levinson, A., K.-C. Wong and K. Bosley. 2000. Response of the lower Chesapeake Bay to

forcing from Hurricane Floyd, *in* Proceedings of the 10th International Biennial Conference on Physics of Estuaries and Coastal Seas, SRAMSOE Report No. 366, C. Friedrichs and A. Valle-Levinson, eds., Virginia Institute of Marine Science, Gloucester Point, VA, 119–122.

Vieira, M.E.C. 1985. Estimates of subtidal volume flux in mid Chesapeake Bay. Estuar. Coast. Shelf Sci., *21,* 411–427.

—— 1986. The meteorologically driven circulation in mid-Chesapeake Bay. J. Mar. Res., *44,* 473–493.

Walters, R.A. 1982. Low-frequency variations in sea level and currents in south San Francisco Bay. J. Phys. Oceanogr., *12,* 658–668.

Walters, R.A. and J.W. Gartner. 1985. Subtidal sea level and current variations in the northern reach of San Francisco Bay. Estuar. Coast. Shelf Sci., *21,* 17–32.

Wang, D.-P. 1979a. Subtidal sea level variations in Chesapeake Bay and relations to atmospheric forcing. J. Phys. Oceanogr., *9,* 413–421.

—— 1979b. Wind driven circulation in the Chesapeake Bay, winter 1975. J. Phys. Oceanogr., *9,* 564–572.

Wang, D.-P. and A.J. Elliott. 1978. Non-tidal variability in the Chesapeake Bay and Potomac River: evidence for non-local forcing. J. Phys. Oceanogr., *8,* 225–232.

Weisberg, R.H. 1976. The nontidal flow in the Providence River of Narragansett Bay: a stochastic approach to estuarine circulation. J. Phys. Oceanogr., *6,* 721–734.

Weisberg, R.H. and W. Sturges. 1976. Velocity observations in the west passage of Narragansett Bay: a partially mixed estuary. J. Phys. Oceanogr., *6,* 345–354.

Wiseman, W.J., Jr., W.W. Schroeder and S.P. Dinnel. 1988. Shelf-estuarine water exchange between the Gulf of Mexico and Mobile Bay, Alabama. Am. Fish. Soc. Symp., *3,* 1–8.

Wong, K.-C. 1994. On the nature of transverse variability in a coastal plain estuary. J. Geophys. Res., *99,* 14,209–14,222.

Wong, K.-C. and R.W. Garvine. 1984. Observations of wind-induced, subtidal variability in the Delaware estuary. J. Geophys. Res., *89,* 10,589–10,597.

Wong, K.-C. and J.E. Moses-Hall. 1998a. The tidal and subtidal variations in the transverse salinity and current distributions across a coastal plain estuary. J. Mar. Res., *56,* 489–517.

—— 1998b. On the relative importance of the remote and local wind effects to the subtidal variability in a coastal plain estuary. J. Geophys. Res., *103*(C9); 18,393–18,404.

Wong, K.-C. and R.E. Wilson. 1984. Observations of low-frequency variability in Great South Bay and relations to atmospheric forcing. J. Phys. Oceanogr., *14,* 1893–1900.

Received: *2 January, 2001;* revised: *14 May, 2001.*